

TwinTrack: Bridging Vision and Contact Physics for Real-Time Tracking of Unknown Dynamic Objects

Wen Yang*, Zhixian Xie*, Xuechao Zhang*, Heni Ben Amor, Shan Lin, Wanxin Jin*

*Intelligent Robotics and Interactive Systems (IRIS) Lab

Arizona State University

Project webpage: <https://irislab.tech/TwinTrack-webpage/>

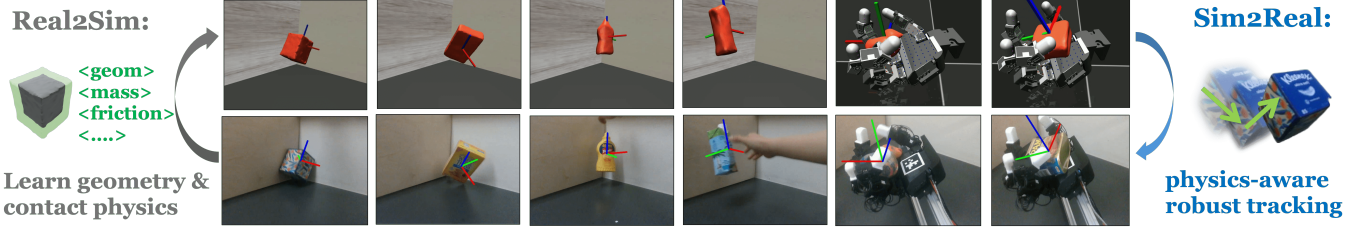


Fig. 1: **TwinTrack** is a physics-aware visual tracking framework for robust, real-time tracking of previously unseen, dynamic objects in contact-rich environments with challenging conditions such as motion blur (Cols. 1–4) or heavy occlusion (Cols. 5–7). The framework integrates two key components: **Real2Sim**, which combines the complementary strengths of vision and contact dynamics to jointly estimate an object’s collision geometry and physical properties; and **Sim2Real**, which performs robust object pose estimation through adaptive fusion of visual tracking and contact dynamics simulation. See [video link](#).

Abstract—Real-time tracking of previously unseen, highly dynamic objects in contact-rich environments—such as during dexterous in-hand manipulation—remains a significant challenge. Purely vision-based tracking often suffers from heavy occlusions due to the frequent contact interactions and motion blur caused by abrupt motion during contact impacts. We propose *TwinTrack*, a physics-aware visual tracking framework that enables robust and real-time 6-DoF pose tracking of unknown dynamic objects in a contact-rich scene by leveraging the contact physics of the observed scene. At the core of *TwinTrack* is an integration of Real2Sim and Sim2Real. In Real2Sim, we combine the complementary strengths of vision and contact physics to estimate object’s collision geometry and physical properties: object’s geometry is first reconstructed from vision, then updated along with other physical parameters from contact dynamics for physical accuracy. In Sim2Real, robust pose estimation of the object is achieved by adaptive fusion between visual tracking and prediction of the learned contact physics. *TwinTrack* is built on a GPU-accelerated, deeply customized physics engine to ensure real-time performance. We evaluate our method on two contact-rich scenarios: object falling with rich contact impacts against the environment, and contact-rich in-hand manipulation. Experimental results demonstrate that, compared to baseline methods, *TwinTrack* achieves significantly more robust, accurate, and real-time 6-DoF tracking in these challenging scenarios, with tracking speed exceeding 20 Hz.

I. INTRODUCTION

Real-time tracking of 6-DoF pose of a previously unseen, highly dynamic unknown object in contact-rich environments is a fundamental step to robotic dexterous manipulation [1]–[3] and physical scene understanding [4]. In contact-rich scenarios, frequent contact interactions between objects, the robot, and the surrounding environment often induce large occlusions and abrupt motion changes (e.g., jumps of object velocities). As a result, purely vision-based tracking [5] can easily struggle due to the degraded and incomplete visual observations.

An approach to overcome those challenges is to integrate contact physics knowledge [6] into the tracking pipeline. Simulated contact interactions and motion, if properly aligned with the real world, can anticipate object poses, helping to compensate for degraded visual tracking, and improving tracking accuracy with physics-informed structures. Furthermore, incorporating contact dynamics also bridges the gap between visual perception and digital physics simulation, enabling downstream applications such as model-based dexterous manipulation control [7]–[9].

However, building a physics-informed tracking system from monocular RGB-D data for unknown objects is challenging, especially in highly dynamic scenes with real-time constraints. Such a system must jointly estimate object pose, geometry, and physical properties (e.g., mass, inertia, friction coefficients) from RGB-D inputs. The high-dimensional optimization space presents major challenges for achieving stable tracking performance. To address such, we expect a modular framework that leverages the interdependencies among components and integrates them cohesively. This must be paired with a GPU-accelerated implementation to achieve low tracking latency.

Toward such a physics-informed tracking system, three major challenges need to be addressed. (i) First, how can visual cues and contact dynamics be efficiently integrated to produce a rich yet collision-accurate geometry? Object geometry is critical for both anchoring object pose estimation [10] and determining collisions in contact physics. While vision offers dense geometric reconstructions, observation noise and occlusion often result in a geometry estimate that deviates from reality. In contrast, geometry learned from contact events are highly accurate, but tend to be sparse and inefficient [11]. Thus, their complementary benefits demand a careful design for efficient integration of the two. (ii) Second, contact interaction—including making and breaking contact, stick-slip transitions, and impacts—introduce

highly non-smooth and sometimes chaotic object motion in the scene. Thus, classic gradient-based dynamics learning and state estimation can suffer due to local and less informative gradients [12]. (iii) Third, achieving real-time tracking performance remains a fundamental obstacle. It requires a highly efficient implementation that tightly integrates physics learning and estimation to enable low-latency and stable tracking.

To address these challenges, we propose *TwinTrack* (Fig. 1), a physics-aware tracking framework that bridges vision and contact physics to enable robust, real-time 6-DoF pose tracking of previously unseen, dynamic objects in contact-rich environments. *TwinTrack* tightly integrates contact dynamics learning with robust object pose estimation via *Real2Sim* and *Sim2Real* submodules. The framework takes as input monocular RGB-D images and, robot proprioceptive data if available, and outputs real-time 6-DoF object poses with resilience to severe motion blur, occlusions, and partial observability. Specifically, *TwinTrack* includes the following novel components:

(I) *Integration between Real2Sim and Sim2Real.* *Real2Sim* focuses on learning object contact geometry and contact dynamics from temporal RGB-D observations. To handle the discontinuous and non-smooth nature of contact interactions, contact dynamics parameters are learned via GPU-parallel, sampling-based optimization. *Sim2Real*, in turn, enables physics-aware tracking of the object’s 6-DoF pose by leveraging the learned contact dynamics, achieving robustness to motion blur, occlusions, and partial observability.

(II) *Geometry estimated from vision and corrected by contact dynamics.* In *Real2Sim*, a dense geometry representation is first extracted from pure visual observation. Due to inherent uncertainty or partial observation in visual data, the obtained geometry is often inaccurate or incomplete for collision-based contact dynamics. To address this, we propose compensating the visual geometry in the next phase of contact dynamics learning, during which other physical properties are also learned. This two-phase process allows us to effectively integrate dense vision and reliable contact cues to derive contact-accurate geometry.

(III) *Real-time implementation.* *Real2Sim* learning and *Sim2Real* tracking are implemented as the backend and frontend of the overall framework, respectively, to ensure that *Real2Sim* does not interfere with the real-time performance of *Sim2Real*. To support accurate collision detection and neural geometry learning within contact dynamics, we developed a deeply customized physics engine based on MJX [13]. All components are GPU-accelerated and optimized to meet real-time constraints and enable high-throughput learning.

We evaluate the *TwinTrack* framework in two challenging contact-rich scenarios: free-falling and in-hand contact-rich manipulation. These settings involve highly dynamic object motion with rapid velocity changes, frequent occlusions, and intermittent and/or sustained contact impacts with the environment or hand. Our method is compared against the state-of-the-art visual-only pose tracker [10]. The results show that with effectively learning of the geometry and physics of the observed contact scenes, *TwinTrack* achieves physically plausible and robust tracking across diverse real-world object geometries in contact-rich scenes, maintaining real-time performance.

II. RELATED WORK

A. Visual Tracking and Geometry Reconstruction

Estimating object pose and geometry using purely visual cues has been a long-standing focus in computer vision community. When provided with strong priors such as CAD models or through online template matching [14]–[17], existing methods can achieve real-time 6D pose tracking with high accuracy. However, dependence on prior knowledge restricts their ability to generalize to unseen objects. Thus, several works explore few-shot generalization [18]–[20], yet they still require reference observations of the object with known camera poses. More recent approaches aim to track previously unseen objects without any prior knowledge, either by integrating pre-trained image descriptors [21] or by jointly learning 3D representations during tracking via neural fields [5], [10]. In parallel, Gaussian splatting has emerged as a powerful representation for object modeling. For example, Dynamic 3D Gaussians [22] track object points by directly optimizing Gaussian poses through a regularized rendering loss, demonstrating impressive performance in dynamic scenes.

While these purely vision-based approaches have achieved notable performance in slow or moderately dynamic conditions [5], [10], [21], they often struggle in highly dynamic, contact-rich scenarios. These scenarios typically involve fast object motion, abrupt motion changes, and frequent occlusion [23], [24], which arise from rich physical interactions between objects, robots, and surrounding environments [25], [26]. In such scenarios, visual observations are often degraded or incomplete, leading to unreliable pose tracking. Moreover, object geometry reconstructed from visual data may be uncertain due to noisy observations. In downstream tasks such as contact-rich manipulation, even subtle inaccuracies in visual geometry can result in significant inconsistencies in motion prediction [11], [27]. These limitations underscore the need to incorporate physical knowledge, such as contact cues and motion dynamics, to enhance robustness and ensure that estimated pose and geometry are physically plausible. Improving the physical validity of perception not only strengthens tracking performance during interaction but also helps reduce the sim-to-real gap, ultimately benefiting applications such as contact-rich manipulation and model-based control [7].

B. Physics-Informed Tracking

A growing body of work explores incorporating physics priors into visual tracking and reconstruction to enforce physical plausibility. In human motion capture, simulation-based constraints [28] and soft physics priors [29]–[31] have been used to regularize tracking for improved realism. These methods often assume known physical properties, such as body mass, shape, ground plane, or contact locations, which can limit its generalization. More recent approaches [25], [32] jointly learn object or scene geometry and physical parameters by minimizing simulation or prediction loss from differentiable simulators, along with differentiable rendering loss.

In a similar vein, [4] proposes a *Real2Sim* framework that extracts collision geometry and physics parameters from robot joint torque sensors and external cameras, relying directly

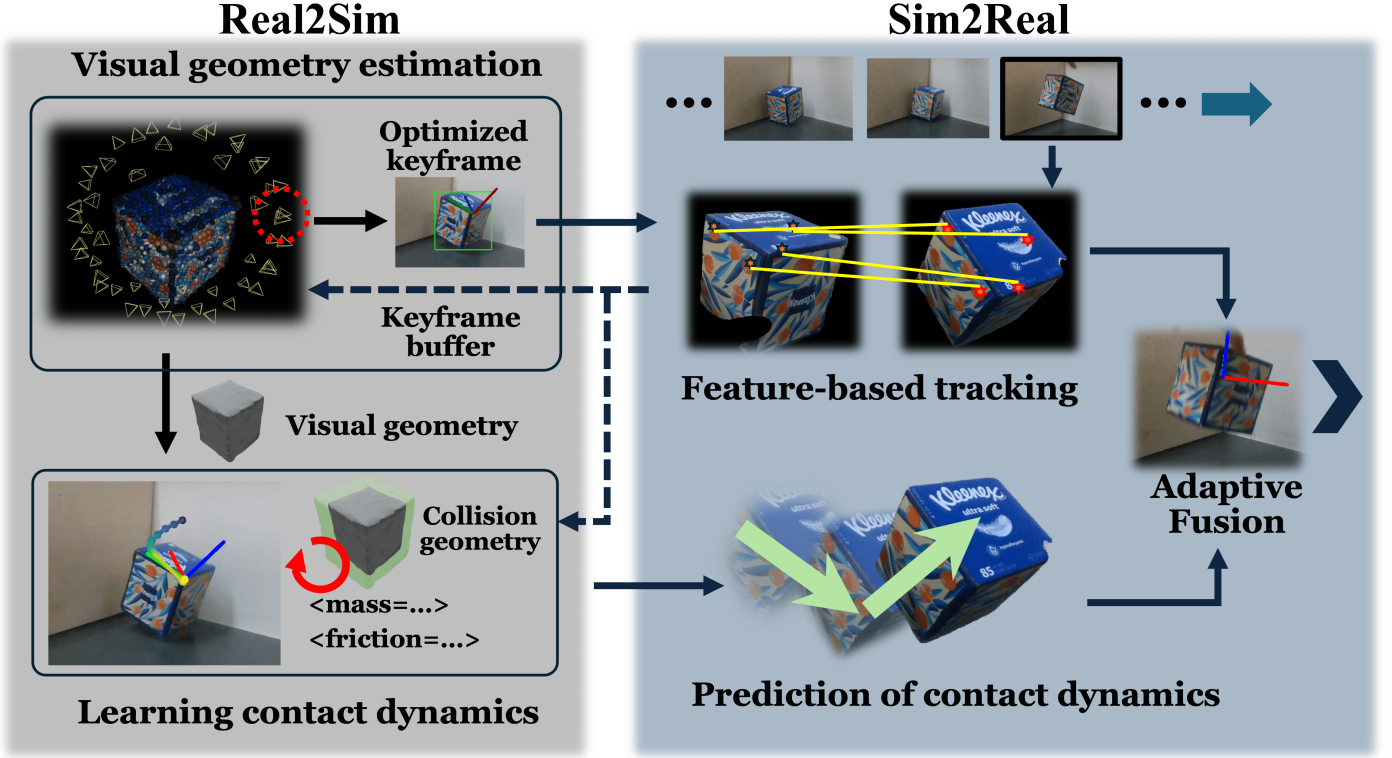


Fig. 2: Overview of **TwinTrack** framework. Our framework includes two main components: **Real2Sim** for learning object geometry and contact physics, and **Sim2Real** for physics-aware real-time pose tracking. In **Real2Sim**, object visual geometry, represented as the Gaussian Splatting model, is obtained from a selection of keyframes by jointly optimizing the geometry and keyframes. The obtained geometry is continually updated in the next phase of learning contact dynamics, together with identifying other physical properties. In **Sim2Real**, feature correspondence is performed for each new frame with respect to an optimized keyframe from **Real2Sim**; meanwhile the learned contact dynamics also predicts the current object pose. The final object pose is an adaptive fusion of both visual tracking and dynamics prediction.

on visual geometry for physics learning. [26] presents a two-stage pipeline that reconstructs a photo-realistic, physically grounded, and real-time interactive digital twin from videos of object interactions, where geometry and dynamics are jointly optimized. However, the motion in their scenarios is relatively slow and smooth. In contact-rich scenes with frequent occlusion and motion blur, visual geometry may be unreliable, potentially degrading dynamics learning and tracking performance in collision-sensitive applications. The most relevant to our work is [33], which combines visual and contact cues to infer geometry under occlusion. However, it focuses on reconstruction rather than real-time tracking, where efficiently integrating vision and contact dynamics remains a key challenge.

C. Learning contact physics

Learning an accurate physics model is essential for improving the physics-informed perception [26], [34], [35], including both pose tracking and geometry reconstruction. However, in real-world, contact interactions are inherently non-smooth and often involve stiff transitions, and this poses significant challenges for learning. Prior studies [11], [36] have shown that standard neural networks struggle to capture such discontinuities, due to their inherent smooth bias [12]. While some differentiable simulators, such as Warp [37] and MJX [38], provide the interface to access the gradient, the gradients, however, are

often discontinuous, local, or biased, which are hard to provide useful information for global optimization [12]. Several studies [7], [9], [12], [39] focus on relaxing the stiff constraint to get smooth approximated gradient. In this work, our method avoids the need for smooth surrogates by adopting a sampling-based optimization strategy that does not rely on contact gradients. Furthermore, by embedding a neural SDF representation of object geometry within the simulator, we enable a learnable compensation mechanism that adjusts contact geometry from observed interactions, enhancing simulation-reality alignment.

III. OVERVIEW OF TWINTRACK FRAMEWORK

A. Problem Statement

We consider a sequence of RGB-D images for a contact-rich dynamic scene, where an unknown, dynamic object frequently makes and breaks contact with a robot and/or surrounding environments such as walls or the ground. We denote the RGB-D image at frame k as (I_k, D_k) where I_k and D_k represent RGB and depth images, respectively. Given the degraded or partial visual observation due to motion blur and occlusion, as discussed previously, TwinTrack aims to robustly and real-time estimate the 6-DoF pose of the object, denoted as \mathbf{q}_k for each frame k . The framework only requires as input monocular RGB-D images and, when available, robot proprioceptive data,

and outputs real-time 6-DoF object poses with resilience to severe motion blur, occlusions, and partial observability.

B. Overview

As shown in Fig. 2, TwinTrack includes two major components: Real2Sim, running in backend, and Sim2Real running as frontend, both of which are described below.

Real2Sim: learning object geometry & contact dynamics (Section IV). Real2Sim is a two-phase process. The first phase estimates the object’s visual geometry from purely visual input through joint optimization of geometry representation and keyframe camera poses. The optimized keyframe poses serve as anchors for visual correspondence in Sim2Real, while the reconstructed geometry is forwarded to the second phase for physics-informed refinement. In the second phase, Real2Sim learns contact dynamics through compensating for gaps in the visual geometry and estimating additional physical parameters, e.g., object mass, inertia, and friction coefficients. The resulting contact dynamics model is then used in Sim2Real to enable physics-aware robust pose tracking.

Sim2Real: physics-aware robust pose tracking (Section V). In Sim2Real, visual correspondence is established by matching features between the current frame and an optimized keyframe from Real2Sim. Simultaneously, the contact dynamics learned from Real2Sim predicts (forward simulates) the object pose for the current frame. The final robust pose estimate is obtained through fast, adaptive fusion of visual correspondence tracking and contact dynamics simulation.

Initialization of TwinTrack: At the initial stage of the framework, both the object geometry and contact dynamics estimated by Real2Sim are unreliable. As a result, the contact dynamics cannot be trusted for physics-informed tracking. To ensure stability during this early stage, Real2Sim relies primarily on visual tracking alone to initialize the system, as indicated by the dashed lines in Fig. 2. After this burn-in period, Real2Sim begins to continuously learn and integrate with Sim2Real, progressively improving the accuracy and robustness of the overall process.

IV. REAL2SIM: LEARNING GEOMETRY AND CONTACT PHYSICS

As shown in Fig. 2, Real2Sim is a two-phase process: object visual geometry is first estimated using a set of keyframes from a keyframe buffer, and then refined during the phase of contact dynamics learning along with identifying other physical property. The inputs to Real2Sim are keyframe buffer and historical tracking data, both of which are from Sim2Real (Section V). The outputs of Real2Sim are the learned contact dynamics and optimized keyframes.

A. Visual Geometry Estimation

The goal of this phase is to estimate the visual geometry of the unknown object from a selection of keyframes, meantime optimizing the poses of the keyframes. The estimated geometry will be used in the contact dynamics for refinement and collision detection, while the optimized keyframes will be used as pose anchors for visual tracking in Sim2Real in Section V-A.

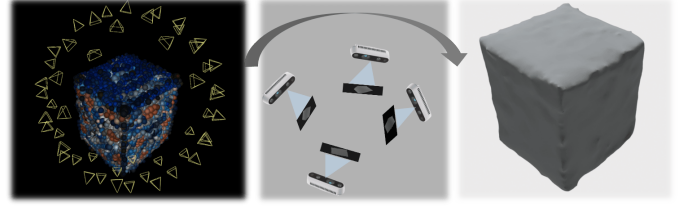


Fig. 3: Visual geometry estimation. Left: joint optimization of Gaussian Splatting (GS) model \mathcal{G}_{gs} and keyframe poses. Middle: depth rendering from the obtained GS model. Right: learning neural SDF $\mathbf{SDF}_{\text{vision}}$ from the rendered depth images.

As shown in Fig. 3, we use the Gaussian Splatting (GS) primitives \mathcal{G}_{gs} [40] to represent the visual model of the object, jointly encoding geometry and appearance. Following [41], we jointly optimize the GS model \mathcal{G}_{gs} and the poses of keyframes $\{\mathbf{q}_i\}_{i \in \mathcal{K}}$ from a keyframe buffer \mathcal{K} (detailed in Section V-A) based on the following loss

$$\min_{\{\mathbf{q}_i\}_{i \in \mathcal{K}}, \mathcal{G}_{\text{gs}}} \sum_{i \in \mathcal{K}} \lambda_{\text{pho}} E_i^{\text{pho}} + (1 - \lambda_{\text{pho}}) E_i^{\text{geo}} \quad (1)$$

with E_i^{pho} the photometric residual and E_i^{geo} the geometric residual for the keyframe i , respectively defined as

$$\begin{aligned} E_i^{\text{pho}} &= \|I(\mathcal{G}_{\text{gs}}, \mathbf{T}(\mathbf{q}_i)) - I_i\|_1, \\ E_i^{\text{geo}} &= \|D(\mathcal{G}_{\text{gs}}, \mathbf{T}(\mathbf{q}_i)) - D_i\|_1, \end{aligned} \quad (2)$$

where $I(\mathcal{G}_{\text{gs}}, \mathbf{T}(\mathbf{q}_i))$ renders the Gaussians \mathcal{G}_{gs} for pose \mathbf{q}_i by α -blending; $D(\mathcal{G}_{\text{gs}}, \mathbf{T}(\mathbf{q}_i))$ is the depth rendering; I_i and D_i is the observed image and depth of keyframe i . For the optimization process and its implementation, we follow [41].

The obtained \mathcal{G}_{gs} can be difficult to be directly integrated in physics engine. Therefore, as the final step in this phase, we learn an neural SDF, denoted as

$$\phi = \mathbf{SDF}_{\text{vision}}(\mathbf{p}) \quad (3)$$

via ray-casting sampling on the rendered depth from the GS model \mathcal{G}_{gs} , as shown in Fig. 3. The obtained $\mathbf{SDF}_{\text{vision}}$ will then be used in contact dynamics in Section IV-B.

B. Contact Dynamics with Compensated Visual Geometry

Our contact dynamics is built on MJX physics engine [38], [42] but with a deep customization of its collision detection pipeline for seamless integration with the neural SDF geometry. Also, its implementation with JAX language [43] allows us to perform GPU-parallel simulation and sampling-based optimization.

In general notation, the contact dynamics in MJX physics engine is formulated as

$$\begin{aligned} \mathbf{M}(\mathbf{q}_k)(\mathbf{v}_{k+1} - \mathbf{v}_k) &= h\mathbf{c}(\mathbf{q}_k, \mathbf{v}_k) + h\mathbf{u}_k + \sum_i \mathbf{J}_i(\mathbf{q}_k)^\top \boldsymbol{\lambda}_i \\ 0 \leq \boldsymbol{\lambda}_i \perp \phi_i(\mathbf{q}_{k+1}) &\geq 0, \quad i \in \mathcal{C}(\mathbf{q}_k, \mathbf{SDF}_{\text{collision}}) \end{aligned} \quad (4)$$

Here, $(\mathbf{q}_k, \mathbf{v}_k)$ is the generalized position and velocity of the contact-rich system (object and robot). h is the time step. $\mathbf{M}(\mathbf{q}_k)$ is the system inertia matrix. $\mathbf{c}(\mathbf{q}_k, \mathbf{v}_k)$ includes all non-contact forces, such as gravity and inertial effects. \mathbf{u}_t is the input force. $\boldsymbol{\lambda}_i$ is the i -th contact impulse (including

friction) between the object and robot/environment and $\mathbf{J}_i(\mathbf{q}_k)$ is the corresponding contact Jacobian. $\mathcal{C}(\mathbf{q}_k, \mathbf{SDF}_{\text{collision}})$ is the collision detection pipeline (described below) at system position \mathbf{q}_k with object collision SDF geometry $\mathbf{SDF}_{\text{collision}}$ (explained below). The second equation is the contact complementarity constraint, with ϕ_i being the “generalized” collision distance. The complementarity intuitively says either the contact impulse λ_i or the contact distance $\phi_i(\mathbf{q}_{k+1})$ is zero, but both cannot be negative. The computed \mathbf{v}_{k+1} (together with λ_i) will be used to integrate to the next position \mathbf{q}_{k+1} based on semi-implicit euler method, denoted as $\mathbf{q}_{k+1} = \mathbf{q}_k \oplus \mathbf{v}_{k+1}$.

In Real2Sim, we make the following modification to MJX physics engine to better integrate with neural geometry and contact dynamics learning.

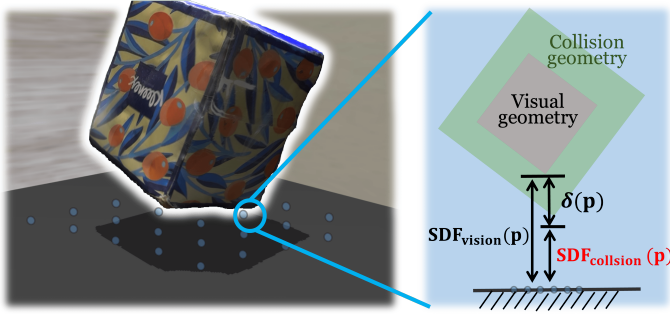


Fig. 4: Collision geometry is a combination of visual geometry plus a learnable geometry compensation.

a) Collision Geometry Compensation: The previously obtained visual geometry $\mathbf{SDF}_{\text{vision}}$ can be imperfect or biased due to noisy or partial observation. If noisy $\mathbf{SDF}_{\text{vision}}$ is directly used in collision detection pipeline, the resulting contact event prediction can deviate from reality, leading to the wrong contact behavior simulation. To address this issue, we propose compensating the visual geometry (3) with a residual term:

$$\mathbf{SDF}_{\text{collision}}(\mathbf{p}) = \mathbf{SDF}_{\text{vision}}(\mathbf{p}) - \delta(\mathbf{p}). \quad (5)$$

Here, we name the residual term $\delta(\mathbf{p})$ as *collision geometry compensation*, which is to compensate for the inaccuracy or bias of visual geometry $\mathbf{SDF}_{\text{vision}}$. This $\delta(\mathbf{p})$ will be learned, along with other physics parameters such as, mass, inertia, and friction coefficient in (4). The compensated geometry, which is called *collision geometry* $\mathbf{SDF}_{\text{collision}}$, will be used in MJX collision detection and simulation.

b) Collision Detection with Neural SDFs: The current MJX physics engine only supports convex meshes or primitive shapes for collision detection. To handle of arbitrary non-convex object geometry represented by $\mathbf{SDF}_{\text{collision}}$, we customize the collision detection pipeline in MJX. The collision detection with SDF geometry follows [7]. Specifically, the collision detection with a SDF geometry is performed by querying $\mathbf{SDF}_{\text{collision}}(\mathbf{p})$ with surface points \mathbf{p} sampled from surrounding entities, such as the ground, walls, or robot fingers, as shown in Fig. 4. With JAX-GPU acceleration, such distance queries can be executed in parallel with minimal computational overhead.

C. Learning Contact Dynamics

The learning of contact dynamics focuses on updating the following parameter in (4):

$$\theta = \{m_{\text{obj}}, \text{diag}[I_x, I_y, I_z]_{\text{obj}}, \mu, \delta\} \quad (6)$$

which includes the object’s mass, diagonalized inertia matrix, friction coefficient, and a collision geometry compensation term (5). The update of contact physics model/engines can be formulated as minimizing the one-step prediction loss

$$\mathcal{L}(\theta) = \sum_{(\mathbf{q}_k, \mathbf{v}_k, \mathbf{q}_{k+1}) \in \mathcal{D}_{\text{tracking}}} \|\mathbf{F}_\theta(\mathbf{q}_k, \mathbf{v}_k) - \mathbf{q}_{k+1}\|_W^2, \quad (24)$$

where $\mathcal{D}_{\text{tracking}}$ is the history tracking data generated from Sim2Real (Section V). \mathbf{F}_θ generically represents the contact dynamics in (4) for notation simplicity. W is the weight matrix to balance the scaling of translational and rotational losses.

Note that in our implementation, while a more expressive residual function $\delta(\mathbf{p})$ could be learned to better capture discrepancies between vision and collision geometries, we adopt a constant value δ . This is due to the inherent sparsity and intermittency of contact events, where directly fine-tuning a more expressive $\delta(\mathbf{q})$, such as neural network, is unstable and prone to overfitting. Instead, we learn a constant geometry compensation parameter δ . This means compensating for minor inaccuracies in the visual geometry by uniformly expanding it by a margin of δ . This provides a lightweight yet effective mechanism to refine contact behavior.

The non-differentiability of contact dynamics introduces challenges when optimizing (24) using gradient-based methods. Although MJX supports differentiable simulation steps, the resulting first-order gradients are limited in local contact modes and fail to provide useful guidance for global optimization [12], [44]. On the other hand, MJX enables highly parallelized simulations across a large number of randomized environments, making it well-suited for sample-based optimization methods. Therefore, we adopt a cross-entropy method (CEM) [45] to solve (24). However, unlike standard CEM variants [45], which update the sampling mean and variance based on the top elite samples, we use an alternative update rule based on softmax-weighted average over all samples, similar to the model-predictive path integral work [46]. Specifically, let the sample size at each iteration be N ; the particles $\theta_i^{(k+1)}$, $i = 1, 2, \dots, N$, at the $(k+1)$ -th iteration is sampled from $\theta_i^{(k+1)} \sim \mathcal{N}(\mu^{(k+1)}, \Sigma)$. Here,

$$\mu^{(k+1)} = \frac{\sum_{i=0}^N \exp(\gamma \mathcal{L}(\theta_i^{(k)})) \theta_i^{(k)}}{\sum_{i=0}^N \exp(\gamma \mathcal{L}(\theta_i^{(k)}))}. \quad (7)$$

Here, the γ is the temperature hyperparameter, and covariance matrix Σ is set as diagonal and constant, with each entry depending on the scale of the corresponding physical parameters. This update has previously been used in [47].

V. SIM2REAL: PHYSICS-AWARE ROBUST TRACKING

As shown in Fig. 2, Sim2Real focuses on robustly and real-time estimate the pose of the object by integrating both feature-based tracking and contact dynamics simulation. The inputs

to Sim2Real are optimized keyframes and the learned contact dynamics, both of which are from Real2Sim (Section IV). The output of Sim2Real is an updated keyframe buffer used for Real2Sim, and the pose of the tracked object at each frame.

A. Feature-Based Pose Estimation

Feature-based pose estimation computes the relative pose between the current frame and an optimized keyframe (i.e., pose anchor), by detecting and matching visual features between the two. The pose anchor is selected as the nearest keyframe, which has been optimized during the Real2Sim process described in Section IV-A. The process largely follows BundleSDF [5], and is briefly summarized below.

a) *Feature Matching*: We first segment the object region in the current frame using SAM2 [48]. We use SAM2 [48] with the prompt given only at the first frame. We adopt the superpoint [49] to extract object feature on current frame and reference keyframe. Each feature includes feature point and descriptor vector. With depth data, the feature point is 3D. After feature extraction, feature matching is performed by LightGlue [50]. Then, a RANSAC-based pose estimator [51] using least squares is also applied to filter wrong feature correspondences.

b) *Keyframe Buffer*: We use keyframe as pose anchor instead of the previous frame, because the latter typically suffers from long-term drift. The keyframe is selected following the setup of [5], [21], and a keyframe buffer \mathcal{K} containing a set of multi-view but sparse keyframes. The poses of those keyframes are continuously optimized in Real2Sim (Section IV-A). To construct keyframe buffer, the first frame is always added. For a new frame tracked, if its rotational geodesic distances against all existing keyframes are larger than a threshold [5], [21], the frame will be added into the keyframe buffer.

c) *Feature-Based Pose Estimation*: For each new frame, its closest keyframe is selected from the keyframe buffer. Given the matched (filtered) features between the current frame and the selected keyframe, the object pose is estimated from this frame pair. Note here, we only use a single frame pair for pose estimation of current frame, instead of optimization over a multi-keyframe pose graph [5], [21]. While a single frame pair is less accurate, it significantly improves tracking speed and is later refined by fusing with contact physics prediction.

B. Physics-Aware Pose Optimization

Object pose estimation at each frame, given feature-based estimation and prediction of the learned contact dynamics, can be treated as a Kalman filtering problem. However, we found such formulation presents practical complexity. For example, Extended Kalman Filter [52] may suffer due to non-smoothness of contact dynamics, and particle filters [53] may incur computational overhead due to large number of forward simulations. Thus, we propose a simple yet effective strategy that adaptively fuses visual tracking with physics predictions for robust and efficient object pose estimation.

For the current frame with index k , we formulate the joint estimation of object pose \mathbf{q}_k as a problem of jointly mini-

mizing the visual correspondence loss and one-step dynamics prediction loss:

$$\min_{\mathbf{q}_k} w_k \mathcal{L}_{\text{vision}}(\mathbf{q}_k) + (1 - w_k) \mathcal{L}_{\text{dynamics}}(\mathbf{q}_k), \quad (8)$$

where $\mathcal{L}_{\text{vision}}(\mathbf{q}_k)$ is the object visual correspondence loss; $\mathcal{L}_{\text{dynamics}}(\mathbf{q}_k)$ is the contact dynamics prediction loss; the weighting parameter $w_t \in [0, 1]$ is balancing the contributions of the two and will be adaptively set based on the quality of visual correspondences. We explain the three terms below.

The object visual correspondence loss $\mathcal{L}_{\text{vision}}(\mathbf{q}_k)$ quantifies the sum of squared distance of matched 3D feature points between the current frame and the selected keyframe (recall Section V-A):

$$\mathcal{L}_{\text{vision}}(\mathbf{q}_k) = \sum_j \left\| \mathbf{T}(\mathbf{q}_k) \mathbf{p}_k^j - \mathbf{T}(\mathbf{q}_n) \mathbf{p}_n^j \right\|_2^2, \quad (9)$$

Here $(\mathbf{p}_k^j, \mathbf{p}_n^j)$ is the j -th matched feature pair from the current frame of pose \mathbf{q}_k and the selected n -th keyframe of the pose \mathbf{q}_n . $\mathbf{T}(\cdot)$ is the operation from pose \mathbf{q} (position and quaternion) to the corresponding transformation matrix. The one-step prediction loss of contact dynamics is defined as

$$\mathcal{L}_{\text{physics}}(\mathbf{q}_k) = \left\| \mathbf{q}_k - \mathbf{F}_{\text{physics}}(\mathbf{q}_{k-1}, \mathbf{v}_{k-1}) \right\|_2^2, \quad (10)$$

Here, $\mathbf{F}_{\text{physics}}$ is the generic notation to (4), which has been learned in Real2Sim in Section IV-B; \mathbf{q}_{k-1} is the robust pose estimate of the previous frame; and \mathbf{v}_{k-1} denotes the velocity at the previous frame, estimated via finite difference on visual pose if visual cues are reliable; otherwise, it is taken from the simulator's dynamics evolution.

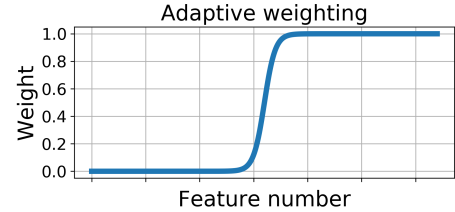


Fig. 5: Adaptive weighting parameter

The weighting $w_t \in [0, 1]$ controls the balance between the physics-based prediction and feature-based estimation. We propose to set w_t adaptively based on the quality of feature matching, which is quantified by the number of the matched feature pairs that remain after filtering (Section V-A). The underlying intuition is that a higher number of reliable feature matches typically indicates favorable visual conditions (e.g., less motion blur or occlusion), and thus the visual estimate should be assigned more weight. We define w_t as a function of the number of matched feature pairs using a sigmoid-like mapping, as shown in Fig. 5.

VI. EXPERIMENTS

We evaluate the TwinTrack framework across a range of contact-rich scenarios. Our evaluation primarily focuses on two core aspects: (1) Real2Sim: how effectively does it learn contact physics dynamics to align and predict the real-world contact-rich motion? and (2) Sim2Real: to what extent does it

enhance tracking robustness in highly dynamic, contact-rich environments? These evaluations are intended to demonstrate TwinTrack’s ability to bridge the sim-to-real gap for robust perception in contact-rich environments.

A. Tasks and Dataset



Fig. 6: Two contact-rich scenarios with different objects.

Our evaluation is centered around two distinct contact-rich scenarios across various objects, as shown in Fig. 6:

Scenario I: Impact-Rich Falling with Motion Blur: The scene consists of two walls and the ground forming a corner, with three orthogonal planar surfaces. Objects are released from human hand with an initial velocity and undergo free fall, eventually colliding with the walls and the ground floor. The key challenge in this case lies in the impact-rich, dynamic nature of object motion. Upon impact with the wall or ground, the object experiences instantaneous impulses that cause abrupt changes in its velocity and direction. It leads to frequent motion blur in the captured frames, making robust pose tracking particularly difficult. In this scenario, we use six everyday objects: snack box, tissue box, milk bottle, Spam can, and 3D-printed duck.

Scenario II: In-Hand Manipulation with Occlusion: A LEAP four-fingered robotic hand [54] manipulates objects in hand with a random policy. The motion involves rich contact between the object and the hand fingers and palm. The primary challenge arises from partial occlusions of the object. The object may undergo abrupt motions, caused by the impact from random finger motion. These factors make tracking difficult. In this scenario, we use the Spam can and 3D-printed duck, as their sizes make them well-suited for handheld interaction.

We collect RGB-D video data using a single-view camera (Intel RealSense D435i) for the above two scenarios with different objects. For Scenario II, we additionally record the robotic hand’s joint states. For each scenario, 4 trajectories under varying motion conditions are collected. Among them, 3 trajectories exhibit relatively mild contact dynamics, involving planar sliding or lateral shaking, and are primarily used for learning contact physics. One trajectory is reserved for evaluation for highly dynamic conditions, including abrupt contact impacts or rapid motion changes, to test the robustness of tracking. The data in Scenario I is collected from free-motion phase, starting after the object is released from human hand.

To obtain ground-truth tracking results for the collected videos, we first offline reconstruct high-quality textured mesh models of all objects using the Scaniverse app [55]. These

mesh models are then used as input to FoundationPose [10], a state-of-the-art 6D pose tracking framework, to generate pseudo ground-truth object poses for all video sequences.

B. Evaluation of Real2Sim

For each scenario and object, Real2Sim learns the contact dynamics using multiple trajectories that involve diverse contact interactions, including bouncing against walls, sliding along the ground, and rich contact in the robot hand.

TABLE I: One-step prediction loss (24) ($100 \times$ position error + quaternion error) of the contact dynamics before and after learning.

	snack box	tissue box	bottle	spam	duck	mustard	LEAP spam	LEAP duck
Before	18.78	9.57	9.82	7.24	5.13	10.18	4.18	23.03
After w/o δ	0.29	0.47	0.87	1.16	0.38	0.56	0.18	0.38
After with δ	0.20	0.22	0.70	0.43	0.21	0.15	0.13	0.28

The contact dynamics learning loss (24) before and after learning is shown in Table I. Here, "Before" is the prediction of a randomly initialized contact dynamics (before Real2Sim learning). The initial model shows a substantial gap from reality, particularly for predicting contact events. For example, simulated objects tend to exhibit exaggerated rebounds or unrealistic sliding behaviors, typically caused by inaccurate mass or inertia estimation. "After w/o δ " corresponds to learning all physical parameters (6) except collision geometry compensation δ (i.e., the contact dynamics uses visual geometry). The learned model reduces the gap but still suffers from inaccurate contact behaviors due to inaccuracy of visual geometry. "After with δ " is the result of learning all parameters (6) including δ . The learned model further lowers the prediction loss, indicating better alignment with visual observations through collision geometry compensation. Although the learned δ may still be imprecise due to camera extrinsic calibration errors, it remains physically plausible, which benefits downstream tracking.

TABLE II: The learned mass of each object versus ground truth.

	snack box	tissue box	bottle	spam	duck	mustard	LEAP spam	LEAP duck
Mass [g]	40	50	24	28	44	65	28	44
Learned	38 ± 3	55 ± 5	32 ± 10	15 ± 5	38 ± 7	46 ± 5	31 ± 5	47 ± 10

Fig. 8 shows the learning convergence of all physical parameters for each object in each scenario. For each object, we conduct five learning trials with different random seeds. The learned mass for each object, compared to the ground-truth, is reported in Table II. Despite the convergence trends, noticeable gaps remain between the learned parameters and the ground-truth values. We speculate that such gap primarily from two aspects. First, some parameters—such as friction and inertia—are weakly observable under the given data, especially when the motion lacks sufficient richness or excitation in the corresponding degrees of freedom. Second, the way contact is handled in MJX, such as point contact and rigid contact, may fundamentally oversimplify the complexity of real-world physical interactions, leading to inherent modeling bias. As a result, learning may converge to a set of physical parameters that fit the observed motion well, even though they deviate

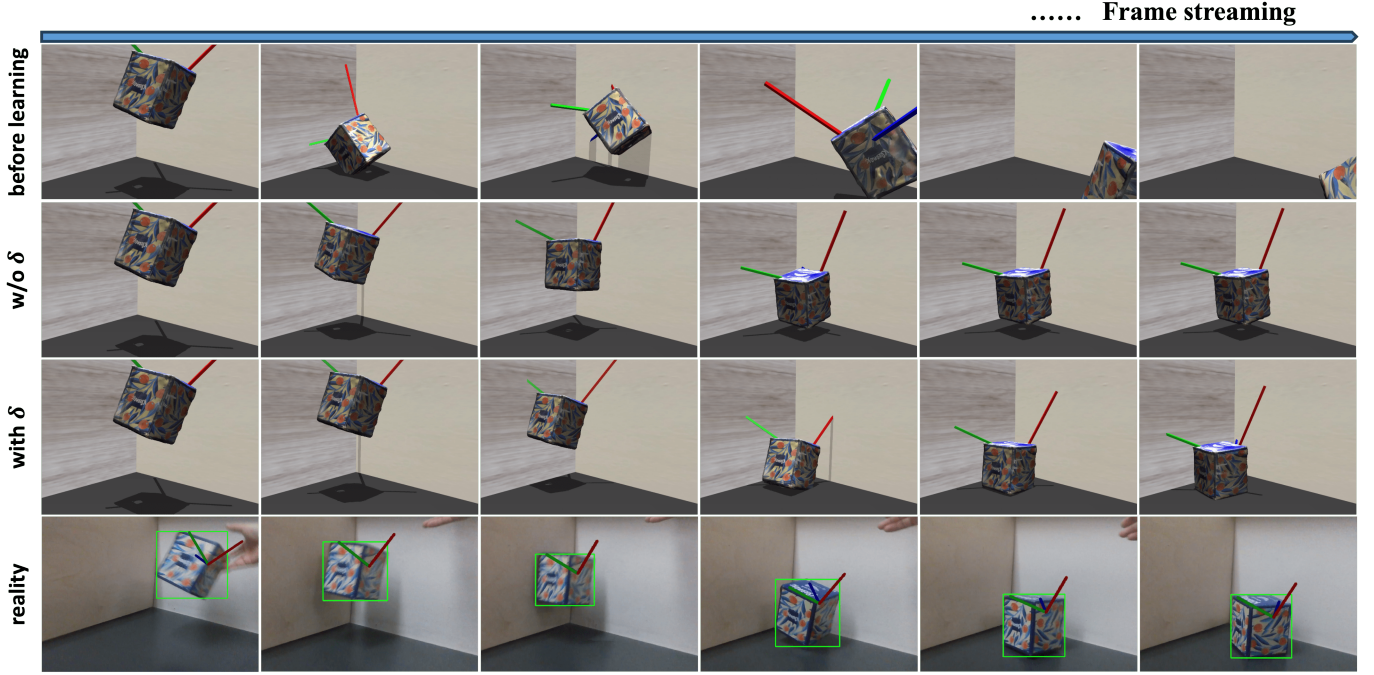


Fig. 7: First row: Open-loop simulation using a random contact dynamics (prior to Real2Sim). Second row: Open-loop simulation of the learned contact dynamics without δ adaptation, i.e., the collision geometry is identical to the visual geometry. Third row: Open-loop simulation of the learned contact dynamics, including the learned collision geometry compensation δ . Fourth row: object’s actual trajectory in real world.

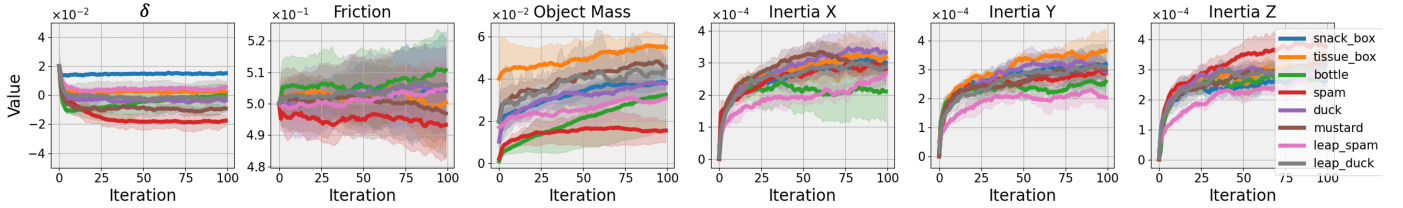


Fig. 8: Convergence of all physics parameters in contact dynamics learning for all objects and tasks. Each learning runs for 5 trials with different random seeds. The solid lines represent the mean values, and the shaded areas indicate the standard deviation across the five trials.

from the true underlying dynamics. We also observe that the learned parameters for the Spam and Duck differ between falling and manipulation scenarios. This discrepancy may be attributed to the mismatch between the simulated robot model and the hardware, as we have not updated the robot’s physical or control parameters in the simulation.

Fig. 7 shows an example of multi-step (open-loop) simulation of contact dynamics for tissue box falling, alongside the real-world video (last row labeled "reality"). The initial position and velocity of simulation are aligned with those in real-world video. The first row ("before learning") shows the simulation of randomly initialized contact dynamics (i.e. before learning). The simulation shows highly unrealistic object motion, such as exaggerated rebounds or missed contact. The second row ("w/o δ ") is the simulation after learning physical parameters (6) except the collision geometry compensation δ . Due to inaccurate visual geometry, contact events has incorrect locations, causing the object to "float" on the surface, degrading contact realism. The third row ("with δ ") shows results after learning all physical parameters including collision geometry compensation δ . The simulated trajectory now closely

resembles the real-world motion in the fourth row, capturing contact onset, rebound, and settling behavior. This demonstrates the effectiveness of Real2Sim in learning collision-accurate geometry and contact dynamics.

Despite a visually appealing alignment of the open-loop simulation with reality in Fig. 7, it should be noted that generally, accurate prediction of long-horizon contact-rich scene is unrealistic due to the chaotic and sensitive nature of contact physics. As in the fourth column of Fig. 7, even minor variations in contact timing or surface geometry can lead to large discrepancies in motion. Also, small perturbations in initial conditions can yield dramatically different outcomes. Like we explained earlier, the inherent model-reality gap and the limited supervision will also contribute to the long-horizon prediction gap. Therefore, while we claim Real2Sim enables the learning of an effective simulation model from visual inputs, it is best suited for one-step or few-step prediction. For longer horizons, it is preferable to integrate the model with real-time visual feedback to continually correct the accumulation of prediction errors, as in our Sim2Real robust tracking below.

TABLE III: Evaluation for Sim2Real robust tracking [cm].

Metrics	Method	snack box	tissue box	bottle	spam	duck	mustard	Leap Spam	Leap Duck	Avg. \pm Std.
ADD \downarrow	Baseline	2.20	2.14	3.58	3.54	2.66	7.13	1.88	1.01	3.01 \pm 1.86
	w/o dynamics	1.54	9.50	20.29	5.83	3.54	4.81	6.75	5.45	7.21 \pm 5.76
	random	>100.0	>100.0	>100.0	>100.0	1.83	2.74	1.70	3.22	>50.0
	w/o δ	1.48	1.05	0.82	0.70	0.89	2.73	1.72	3.11	1.56 \pm 0.91
	Proposed	1.37	1.04	0.78	0.67	0.83	2.62	1.67	0.87	1.23\pm0.65
ADD-S \downarrow	Baseline	1.12	1.11	1.45	1.73	1.36	1.26	0.81	0.41	1.15 \pm 0.40
	w/o dynamics	0.78	2.50	12.24	1.26	1.28	2.06	2.12	1.61	2.98 \pm 3.78
	random	>100.0	>100.0	>100.0	>100.0	0.89	1.32	0.77	1.19	>50.0
	w/o δ	0.79	0.55	0.40	0.34	0.49	1.31	0.77	1.31	0.74 \pm 0.38
	Proposed	0.74	0.54	0.39	0.33	0.39	1.25	0.75	0.39	0.59\pm0.31

C. Evaluation of Sim2Real

We evaluate the Sim2Real for robust tracking of objects in the two scenarios. The ADD and ADD-S metrics [cm] are used to assess tracking accuracy. The results for all evaluated methods are reported in Table III. Ground-truth poses are obtained from FoundationPose [10], with high-quality textured mesh models obtained in offline and static conditions with Scaniverse software. For comparison, we include a baseline, which is model-free tracking using same method [10] but fed with the same set of keyframes utilized in our Real2Sim.

In addition, we perform three ablation studies to systematically assess the contributions of different designs in our framework. The "w/o dynamics" variant replaces the contact dynamics model with a simplified constant-velocity prior, resulting in a vision-only tracking baseline. The "random" variant employs a contact dynamics with random physical parameters for motion prediction. The "w/o δ " variant corresponds to learning all physical parameters in Real2Sim except δ , i.e., keeping the collision geometry the same as visual geometry. The "proposed" method corresponds to learning of all physical parameters including δ in Real2Sim.

Table III shows that the proposed method achieves the best overall performance across all scenarios and objects. By learning contact physics and collision geometry compensation δ , it significantly outperforms all ablated variants. Both baseline and "w/o dynamics" variant rely purely on visual tracking without incorporating contact physics. As a result, their performance is limited under challenging conditions such as motion blur and occlusions. Although "w/o dynamics" variant introduces a constant-velocity prior to help tracking, it lacks the capability to predict contact interactions, resulting in drift and tracking errors when objects interacts with the environment. The "w/o δ " and "proposed" variants highlight the importance of accurate collision geometry in improving physics-aware tracking. The learned collision geometry compensation δ effectively corrects errors in the visual geometry. This leads to a more accurate contact dynamics and therefore higher Sim2Real tracking performance.

The tracking time cost for each module is summarised as follows. Experiments are conducted on a PC with a Ryzen 5955WX CPU and an RTX 4090 GPU. For each frame, SAM2-based segmentation takes approximately 12ms, and SuperPoint feature detection takes around 8ms. The contact dynamics simulation step with neural SDF collision, accelerated via Just-

in-time compilation, completes in 5ms. Keyframe selection and LightGlue matching consume approximately 15ms, while the adaptive fusion optimization step adds an additional 5ms. Other operations take about 3ms. In total, the system can achieve a processing rate of over 20Hz, enabling real-time performance for dynamics tracking. See [video link](#).

VII. CONCLUSION

In this work, we present TwinTrack, a physics-aware tracking framework by bridging visual observations and contact physics to enable robust tracking of unknown dynamic objects in contact-rich environments. TwinTrack includes two major components: Real2Sim, which builds a contact dynamics model from visual observations through estimating and refining object geometry and identifying physical properties; and Sim2Real, which then uses the learned contact dynamics to enhance the robustness and accuracy of 6-DoF pose visual tracking. The evaluation on contact-rich dataset demonstrates robust and real-time performance of the proposed framework against occlusion and motion blur in highly dynamic contact-rich environments.

REFERENCES

- [1] Allison M Okamura, Niels Smaby, and Mark R Cutkosky. An overview of dexterous manipulation. In *Proceedings 2000 ICRA. Millennium Conference. IEEE International Conference on Robotics and Automation. Symposia Proceedings (Cat. No. 00CH37065)*, volume 1, pages 255–262. IEEE, 2000.
- [2] OpenAI: Marcin Andrychowicz, Bowen Baker, Maciek Chociej, Rafal Jozefowicz, Bob McGrew, Jakub Pachocki, Arthur Petron, Matthias Plappert, Glenn Powell, Alex Ray, et al. Learning dexterous in-hand manipulation. *The International Journal of Robotics Research*, 39(1):3–20, 2020.
- [3] Aravind Rajeswaran, Vikash Kumar, Abhishek Gupta, Giulia Vezzani, John Schulman, Emanuel Todorov, and Sergey Levine. Learning complex dexterous manipulation with deep reinforcement learning and demonstrations. *arXiv preprint arXiv:1709.10087*, 2017.
- [4] Nicholas Pfaff, Evelyn Fu, Jeremy Binagia, Phillip Isola, and Russ Tedrake. Scalable real2sim: Physics-aware asset generation via robotic pick-and-place setups. *arXiv preprint arXiv:2503.00370*, 2025.
- [5] Bowen Wen, Jonathan Tremblay, Valts Blukis, Stephen Tyree, Thomas Müller, Alex Evans, Dieter Fox, Jan Kautz, and Stan Birchfield. Bundlesdf: Neural 6-dof tracking and 3d reconstruction of unknown objects. In *Proceedings of the IEEE/CVF Conference on Computer Vision and Pattern Recognition*, pages 606–617, 2023.
- [6] Friedrich Pfeiffer and Christoph Glocker. *Multibody dynamics with unilateral contacts*, volume 421. Springer science & business media, 2000.
- [7] Wen Yang and Wanxin Jin. Contactsdf: Signed distance functions as multi-contact models for dexterous manipulation. *IEEE Robotics and Automation Letters*, 10(5):4212–4219, 2025.

- [8] Wanxin Jin and Michael Posa. Task-driven hybrid model reduction for dexterous manipulation. *IEEE Transactions on Robotics*, 40:1774–1794, 2024.
- [9] Wanxin Jin. Complementarity-free multi-contact modeling and optimization for dexterous manipulation. *Robotics: Science and Systems*, 2025.
- [10] Bowen Wen, Wei Yang, Jan Kautz, and Stan Birchfield. Foundationpose: Unified 6d pose estimation and tracking of novel objects. In *Proceedings of the IEEE/CVF Conference on Computer Vision and Pattern Recognition*, pages 17868–17879, 2024.
- [11] Samuel Pfrommer, Mathew Halm, and Michael Posa. Contactnets: Learning discontinuous contact dynamics with smooth, implicit representations. In Jens Kober, Fabio Ramos, and Claire Tomlin, editors, *Proceedings of the 2020 Conference on Robot Learning*, volume 155 of *Proceedings of Machine Learning Research*, pages 2279–2291. PMLR, 16–18 Nov 2021.
- [12] Hyung Ju Suh, Max Simchowitz, Kaiqing Zhang, and Russ Tedrake. Do differentiable simulators give better policy gradients? In *International Conference on Machine Learning*, pages 20668–20696. PMLR, 2022.
- [13] DeepMind Google. Mujoco-xla (mjx). <https://github.com/google-deepmind/mujoco/tree/main/mjx>, 2025.
- [14] Yann Labbé, Justin Carpentier, Mathieu Aubry, and Josef Sivic. Cosypose: Consistent multi-view multi-object 6d pose estimation. In *Computer Vision–ECCV 2020: 16th European Conference, Glasgow, UK, August 23–28, 2020, Proceedings, Part XVII 16*, pages 574–591. Springer, 2020.
- [15] Yann Labbé, Lucas Manuelli, Arsalan Mousavian, Stephen Tyree, Stan Birchfield, Jonathan Tremblay, Justin Carpentier, Mathieu Aubry, Dieter Fox, and Josef Sivic. Megapose: 6d pose estimation of novel objects via render & compare. *arXiv preprint arXiv:2212.06870*, 2022.
- [16] Martin Sundermeyer, Zoltan-Csaba Marton, Maximilian Durner, Manuel Brucker, and Rudolph Triebel. Implicit 3d orientation learning for 6d object detection from rgb images. In *Proceedings of the european conference on computer vision (ECCV)*, pages 699–715, 2018.
- [17] He Wang, Srinath Sridhar, Jingwei Huang, Julien Valentin, Shuran Song, and Leonidas J Guibas. Normalized object coordinate space for category-level 6d object pose and size estimation. In *Proceedings of the IEEE/CVF conference on computer vision and pattern recognition*, pages 2642–2651, 2019.
- [18] Keunhong Park, Arsalan Mousavian, Yu Xiang, and Dieter Fox. Latent-fusion: End-to-end differentiable reconstruction and rendering for unseen object pose estimation. In *Proceedings of the IEEE/CVF conference on computer vision and pattern recognition*, pages 10710–10719, 2020.
- [19] Yuan Liu, Yilin Wen, Sida Peng, Cheng Lin, Xiaoxiao Long, Taku Komura, and Wenping Wang. Gen6d: Generalizable model-free 6-dof object pose estimation from rgb images. In *European Conference on Computer Vision*, pages 298–315. Springer, 2022.
- [20] Jiaming Sun, Zihao Wang, Siyu Zhang, Xingyi He, Hongcheng Zhao, Guofeng Zhang, and Xiaowei Zhou. Onepose: One-shot object pose estimation without cad models. In *Proceedings of the IEEE/CVF Conference on Computer Vision and Pattern Recognition*, pages 6825–6834, 2022.
- [21] Bowen Wen and Kostas Bekris. Bundltrack: 6d pose tracking for novel objects without instance or category-level 3d models. In *2021 IEEE/RSJ International Conference on Intelligent Robots and Systems (IROS)*, pages 8067–8074. IEEE, 2021.
- [22] Jonathon Luiten, Georgios Kopanas, Bastian Leibe, and Deva Ramanan. Dynamic 3d gaussians: Tracking by persistent dynamic view synthesis. In *2024 International Conference on 3D Vision (3DV)*, pages 800–809. IEEE, 2024.
- [23] Alex Bewley, Zongyuan Ge, Lionel Ott, Fabio Ramos, and Ben Upcroft. Simple online and realtime tracking. In *2016 IEEE International Conference on Image Processing (ICIP)*, pages 3464–3468, 2016.
- [24] Jinkun Cao, Jiangmiao Pang, Xinshuo Weng, Rawal Khirdkar, and Kris Kitani. Observation-centric sort: Rethinking sort for robust multi-object tracking. In *Proceedings of the IEEE/CVF Conference on Computer Vision and Pattern Recognition (CVPR)*, pages 9686–9696, June 2023.
- [25] Gengshan Yang, Shuo Yang, John Z Zhang, Zachary Manchester, and Deva Ramanan. Ppr: Physically plausible reconstruction from monocular videos. In *Proceedings of the IEEE/CVF International Conference on Computer Vision*, pages 3914–3924, 2023.
- [26] Hanxiao Jiang, Hao-Yu Hsu, Kaifeng Zhang, Hsin-Ni Yu, Shenlong Wang, and Yunzhu Li. Phystwin: Physics-informed reconstruction and simulation of deformable objects from videos. *arXiv preprint arXiv:2503.17973*, 2025.
- [27] Wei-Cheng Huang, Alp Aydinoglu, Wanxin Jin, and Michael Posa. Adaptive contact-implicit model predictive control with online residual learning. In *2024 IEEE International Conference on Robotics and Automation (ICRA)*, pages 5822–5828. IEEE, 2024.
- [28] Erik Gärtner, Mykhaylo Andriluka, Erwin Coumans, and Cristian Sminchisescu. Differentiable dynamics for articulated 3d human motion reconstruction. In *Proceedings of the IEEE/CVF conference on computer vision and pattern recognition*, pages 13190–13200, 2022.
- [29] Davis Rempe, Leonidas J Guibas, Aaron Hertzmann, Bryan Russell, Ruben Villegas, and Jimei Yang. Contact and human dynamics from monocular video. In *Computer Vision–ECCV 2020: 16th European Conference, Glasgow, UK, August 23–28, 2020, Proceedings, Part V 16*, pages 71–87. Springer, 2020.
- [30] Soshi Shimada, Vladislav Golyanik, Weipeng Xu, and Christian Theobalt. Physcap: Physically plausible monocular 3d motion capture in real time. *ACM Transactions on Graphics (ToG)*, 39(6):1–16, 2020.
- [31] Minh Vo, Yaser Sheikh, and Srinivasa G Narasimhan. Spatiotemporal bundle adjustment for dynamic 3d human reconstruction in the wild. *IEEE Transactions on Pattern Analysis and Machine Intelligence*, 44(2):1066–1080, 2020.
- [32] John Z Zhang, Shuo Yang, Gengshan Yang, Arun L Bishop, Swaminathan Gurumurthy, Deva Ramanan, and Zachary Manchester. Slomo: A general system for legged robot motion imitation from casual videos. *IEEE Robotics and Automation Letters*, 8(11):7154–7161, 2023.
- [33] Bibit Bianchini, Minghan Zhu, Mengti Sun, Bowen Jiang, Camillo J Taylor, and Michael Posa. Vysics: Object reconstruction under occlusion by fusing vision and contact-rich physics. *arXiv preprint arXiv:2504.18719*, 2025.
- [34] Jad Abou-Chakra, Krishan Rana, Feras Dayoub, and Niko Suenderhauf. Physically embodied gaussian splatting: A realtime correctable world model for robotics. In *8th Annual Conference on Robot Learning*, 2024.
- [35] Licheng Zhong, Hong-Xing Yu, Jiajun Wu, and Yunzhu Li. Reconstruction and simulation of elastic objects with spring-mass 3d gaussians. *European Conference on Computer Vision (ECCV)*, 2024.
- [36] Mihir Parmar, Mathew Halm, and Michael Posa. Fundamental challenges in deep learning for stiff contact dynamics. In *2021 IEEE/RSJ International Conference on Intelligent Robots and Systems (IROS)*, pages 5181–5188. IEEE, 2021.
- [37] Miles Macklin. Warp: A high-performance python framework for gpu simulation and graphics. <https://github.com/nvidia/warp>, March 2022. NVIDIA GPU Technology Conference (GTC).
- [38] Emanuel Todorov, Tom Erez, and Yuval Tassa. Mujoco: A physics engine for model-based control. In *2012 IEEE/RSJ international conference on intelligent robots and systems*, pages 5026–5033. IEEE, 2012.
- [39] Taylor Howell, Simon Le Cleac’h, Jan Bruedigam, Zico Kolter, Mac Schwager, and Zachary Manchester. Dojo: A differentiable physics engine for robotics. *arXiv preprint arXiv:2203.00806*, 2022.
- [40] Bernhard Kerbl, Georgios Kopanas, Thomas Leimkühler, and George Drettakis. 3d gaussian splatting for real-time radiance field rendering. *ACM Trans. Graph.*, 42(4):139–1, 2023.
- [41] Hidenobu Matsuki, Riku Murai, Paul HJ Kelly, and Andrew J Davison. Gaussian splatting slam. In *Proceedings of the IEEE/CVF Conference on Computer Vision and Pattern Recognition*, pages 18039–18048, 2024.
- [42] C. Daniel Freeman, Erik Frey, Anton Raichuk, Sertan Girgin, Igor Mordatch, and Olivier Bachem. Brax - a differentiable physics engine for large scale rigid body simulation, 2021.
- [43] James Bradbury, Roy Frostig, Peter Hawkins, Matthew James Johnson, Chris Leary, Dougal Maclaurin, George Nectala, Adam Paszke, Jake VanderPlas, Skye Wanderman-Milne, and Qiao Zhang. JAX: composable transformations of Python+NumPy programs, 2018.
- [44] Rika Antonova, Jingyun Yang, Krishna Murthy Jatavallabhula, and Jeannette Bohg. Rethinking optimization with differentiable simulation from a global perspective. In *Conference on Robot Learning*, pages 276–286. PMLR, 2023.
- [45] Reuven Y Rubinfeld and Dirk P Kroese. *The cross-entropy method: a unified approach to combinatorial optimization, Monte-Carlo simulation and machine learning*. Springer Science & Business Media, 2004.
- [46] Grady Williams, Paul Drews, Brian Goldfain, James M. Rehg, and Evangelos A. Theodorou. Aggressive driving with model predictive path integral control. In *2016 IEEE International Conference on Robotics and Automation (ICRA)*, pages 1433–1440, 2016.
- [47] Anusha Nagabandi, Kurt Konolige, Sergey Levine, and Vikash Kumar. Deep dynamics models for learning dexterous manipulation. In *Conference on robot learning*, pages 1101–1112. PMLR, 2020.
- [48] Nikhila Ravi, Valentin Gabeur, Yuan-Ting Hu, Ronghang Hu, Chaitanya Ryali, Tengyu Ma, Haitham Khedr, Roman Rädle, Chloe Rolland, Laura Gustafson, Eric Mintun, Junting Pan, Kalyan Vasudev Alwala, Nicolas Carion, Chao-Yuan Wu, Ross Girshick, Piotr Dollár, and Christoph

- Feichtenhofer. Sam 2: Segment anything in images and videos. *arXiv preprint arXiv:2408.00714*, 2024.
- [49] Daniel DeTone, Tomasz Malisiewicz, and Andrew Rabinovich. Superpoint: Self-supervised interest point detection and description. In *2018 IEEE/CVF Conference on Computer Vision and Pattern Recognition Workshops (CVPRW)*, pages 337–33712, 2018.
 - [50] Philipp Lindenberger, Paul-Edouard Sarlin, and Marc Pollefeys. Light-Glue: Local Feature Matching at Light Speed. In *ICCV*, 2023.
 - [51] Konstantinos G Derpanis. Overview of the ransac algorithm. *Image Rochester NY*, 4(1):2–3, 2010.
 - [52] Simon J Julier and Jeffrey K Uhlmann. New extension of the kalman filter to nonlinear systems. In *Signal processing, sensor fusion, and target recognition VI*, volume 3068, pages 182–193. Spie, 1997.
 - [53] Eric A Wan and Rudolph Van Der Merwe. The unscented kalman filter for nonlinear estimation. In *Proceedings of the IEEE 2000 adaptive systems for signal processing, communications, and control symposium (Cat. No. 00EX373)*, pages 153–158. Ieee, 2000.
 - [54] Kenneth Shaw, Ananye Agarwal, and Deepak Pathak. Leap hand: Low-cost, efficient, and anthropomorphic hand for robot learning. *Robotics: Science and Systems (RSS)*, 2023.
 - [55] Inc Niantic. Scaniverse: 3d scanner app. <https://scaniverse.com/>, 2025.